NANO LETTERS

Letter

pubs.acs.org/NanoLett

Switchable Coupling of Vibrations to Two-Electron Carbon-Nanotube Quantum Dot States

P. Weber,[†,‡,⊥] H. L. Calvo,[§,‡,#] J. Bohle,[§,‡] K. Goß,[∥,‡,▽] C. Meyer,[∥,‡] M. R. Wegewijs,[∥,§,‡] and C. Stampfer*[,†,‡,∥]

[†]2nd Institute of Physics, RWTH Aachen University, 52056 Aachen, Germany

[‡]JARA − Fundamentals of Future Information Technology, [§]Institute for Theory of Statistical Physics, RWTH Aachen University, 52074 Aachen, Germany

[∥]Peter Grünberg Institute, Forschungszentrum Jülich, 52425 Jülich, Germany

[⊥]ICFO-Institut de Ciencies Fotoniques, Mediterranean Technology Park, 08860 Castelldefels, Barcelona, Spain

[#]Instituto de Física Enrique Gaviola (IFEG-CONICET) and FaMAF, Universidad Nacional de Córdoba, Ciudad Universitaria, 5000 Córdoba, Argentina

[▽]Physikalisches Institut, Universität Stuttgart, Pfaffenwaldring 57, Stuttgart, Germany

Supporting Information

ABSTRACT: We report transport measurements on a quantum dot in a partly suspended carbon nanotube. Electrostatic tuning allows us to modify and even switch "on" and "off" the coupling to the quantized stretching vibration across several charge states. The magnetic-field dependence indicates that only the two-electron spin-triplet excited state couples to the mechanical motion, indicating mechanical coupling to both the valley degree of freedom and the exchange interaction, in contrast to standard models.

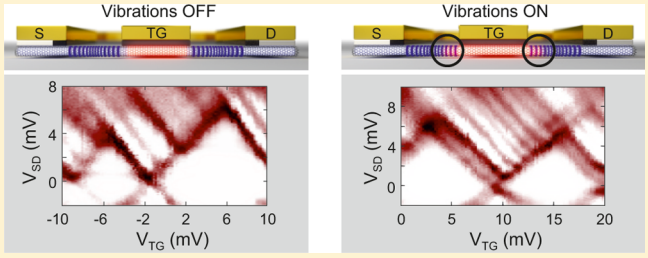

KEYWORDS: *Carbon nanotube, quantum dot, electron transport, nanoelectromechanical systems (NEMS), electron-phonon coupling in low-dimensional structures, spin states*

Carbon nanotubes are found to be an ideal playground for nanoelectromechanical systems (NEMS) because their high-quality, quantum-confined electronic states are accessible by transport spectroscopic techniques and couple strongly to the excitations of different mechanical modes. The growing interest in NEMS is fueled by the desire to accurately sense small masses and forces,[1] address quantum-limited mechanical motion,[2] and integrate such functionality into complex hybrid devices,[3] leading to new applications.[4] The central question is the strength of the coupling of electronic states to the vibrational modes. Whereas molecular junctions display such modes also in electrically gated transport measurements,[5−7] carbon nanotube (CNT) quantum dots allow for a much more viable fabrication, higher mechanical *Q*-factors, and better tuneability as NEMS.[8−13] Also, the coupling to the bending mode can be combined[14,15] with the spin−orbit (SO) interaction[16,17] by making use of the recently demonstrated[11] curvature-induced SO-coupling in CNTs.[18] Whereas the frequency of the vibrational modes has been demonstrated to be tunable,[19−21] another desirable feature is the ability to switch "on" and "off" the electron-vibration coupling in the same device, for example, in envisioned quantum-information processing schemes.[15,22] This is also helpful for fundamental studies of systems in which mechanical motion is combined with other degrees of freedom, for example, the spin[23] and the valley.[24]

Recently, switchable coupling to a classical flexural mode of a CNT has been demonstrated.[12] In this Letter, we present a CNT quantum dot NEMS with a coupling of the electronic states to a longitudinal stretching vibration of about 200 GHz that can be turned "on" and "off". We illustrate the advantage of this by transport measurements in the two-electron quantum-dot regime and find that the well-known Anderson−Holstein scenario breaks down in an unexpected way: different spin states exhibit different coupling strengths to the vibrational mode.

In Figure 1a we show a schematic of a typical suspended CNT quantum-dot device whose scanning electron microscope image is shown in Figure 1b. The CNT is electrically and mechanically connected to both source (s) and drain (d) contacts where the central electrode acts as a suspended, doubly clamped top gate (tg). The quantum dot is formed in the small band gap CNT by the electrostatic potentials of the top and back gate (bg), see Figures 1a and 2a, allowing for

Received: February 25, 2015
Revised: May 27, 2015
Published: June 10, 2015

DOI: 10.1021/acs.nanolett.5b00765
Nano Lett. 2015, 15, 4417−4422

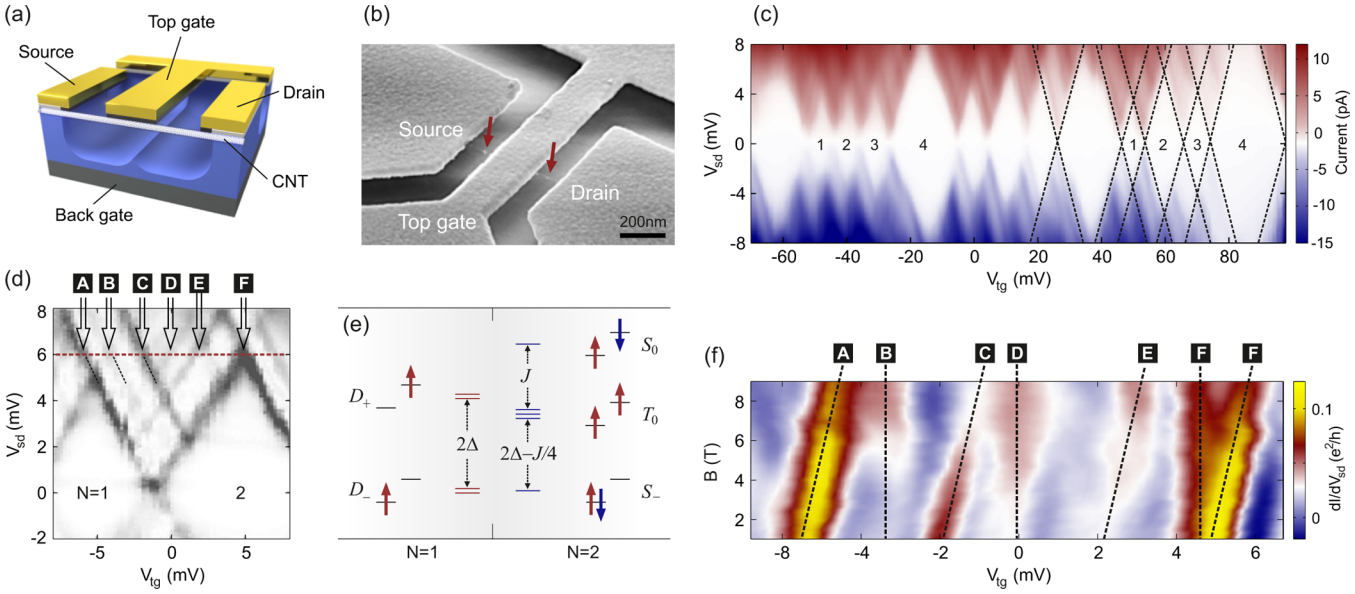

Figure 1. Carbon nanotube quantum dot characterization. (a) Schematic illustration of the cross-section of a partly suspended CNT connected to source and drain electrodes (5 nm Cr, 50 nm Au). While the back-gate shifts the entire potential of the whole structure, the top-gate bridge overlaps with a 200 nm part of the CNT by an oxidized Cr layer, see Supporting Information. (b) Scanning electron-microscopy image of a partly suspended CNT sample. The CNT is just visible and indicated by red arrows. (c) Source-drain current through the quantum dot at zero magnetic field as a function of the bias (V_{sd}) and top-gate voltage (V_{tg}), adjusting the back-gate voltage V_{bg} simultaneously to keep the average chemical potential in the leads constant: $V_{bg} = 4.35\ \mathrm{V} - 0.7 \times V_{tg}$. (d) dI/dV_{sd} at zero magnetic field centered around the $1 \leftrightarrow 2$ single-electron tunneling regime for back-gate voltage $V_{bg} = 4.25$ V in the hole regime. We count the number of electrons relative to the last filled conduction band shell of the CNT as usual. The diagonal dashed lines marked A–F correspond to transitions between the $N = 1$ and 2 electron quantum-dot states. (e) Energy diagram of the one- and two-electron quantum dot states involving the first orbital shell and the corresponding orbital fillings discussed in the text. These states are responsible for the transitions A ($D_- \leftrightarrow S_-$), B ($D_- \leftrightarrow T_0$) and C ($D_- \leftrightarrow S_0$) which are the most relevant ones for the present discussion, see also Supporting Information. For panel (d) we extract $\Delta = 0.8$ meV and $J = 1.2$ meV. (f) Measured magnetic field dependence of the electronic excitation lines along the horizontal line in panel (d) at $V_{sd} = 6$ mV. This way of plotting (see Supporting Information) focuses the attention on the important triplet states by making the transition B into the lowest triplet appear as a vertical line.

electrostatic control of the size of the quantum dot in the range of 250–350 nm, see Supporting Information. By changing the gate voltages we can modify the position and size of the dot with respect to the suspended vibrating region of the CNT, which is a crucial part of our experiment. The high quality of our CNT sample is revealed by the observation of well-resolved, multiple 4-fold shell-structure of the electronic states in the stability diagram in Figure 1c measured at zero magnetic field and at a base temperature of 1.6 K. This shell-structure stems from the combined spin and valley degeneracies in clean CNTs[25−27] and enables a first characterization of the electronic properties by the Coulomb and confinement energies. Importantly, the resulting estimates show that the quantum dot formed in the CNT is comparable to or even larger in size than the top-gate, see Supporting Information.

The key advantage of our device in contrast to previous ones is that we can first obtain detailed information about the electronic spectrum by measuring the differential conductance in a gate voltage regime without signatures of vibrational excitations. For example, in the spectrum shown in Figure 1d the low-energy excitations indicated by dashed black lines can be assigned to transitions between states with electron number $N = 1$ and 2, respectively. These are indicated in the schematic in Figure 1e which shows for $N = 1$ two spin doublets denoted D_- and D_+, obtained by filling the (anti)bonding orbitals $|\pm\rangle = (|K\rangle \pm |K'\rangle)/\sqrt{2}$ of the K and K' valleys with one electron, which are split in energy by 2Δ due to the valley-mixing Δ. For $N = 2$, we have spin-singlets S_- and S_+ (latter not shown) completely filling one of these orbitals, and a singlet S_0 and a triplet T_0 in which two different orbitals are filled. Here the labels of the many-body states S, D, T indicate the spin multiplicities (singlet, doublet, triplet), whereas the subscripts indicate the relevant orbital polarizations. In the transport data of Figure 1d we identify a ground singlet (S_-), an excited triplet (T_0) and another singlet (S_0), split by the exchange energy J. The measured magnetic field transport spectroscopy in Figure 1f confirms this assignment: the slope of the lines A and C for transitions to S_- and S_0, respectively, differs by the Zeeman spin splitting from the slope of line B for the transition to the triplet T_0. We note that for these parameters the singlet S_+ is the highest in energy in Figure 1e. It is not shown there nor discussed further below because this state does not influence the measured transport in the considered regime.[28] Our calculations below do, however, include the state S_+ and confirm that it has negligible influence.

By independently tuning the top- and back gate voltages we can change the electrostatic confinement of the quantum dot and thereby effectively operate a single quantum dot system that can be made sensitive to the vibrating part of the CNT, as illustrated in Figure 2a. The resulting electronic stability diagram in Figure 2b, showing nearly parallel lines, indicates that we can independently fix the electron number in the dot while modifying its shape, dimensions, and position. When measuring the Coulomb diamonds along the lines indicated in Figure 2b one expects, electronically speaking, no qualitative difference. Indeed, along the initial working line marked as (1) in Figure 2b, the measurement in Figure 2c shows no indications of vibrations. However, when tuning to the working

DOI: 10.1021/acs.nanolett.5b00765
Nano Lett. 2015, 15, 4417–4422

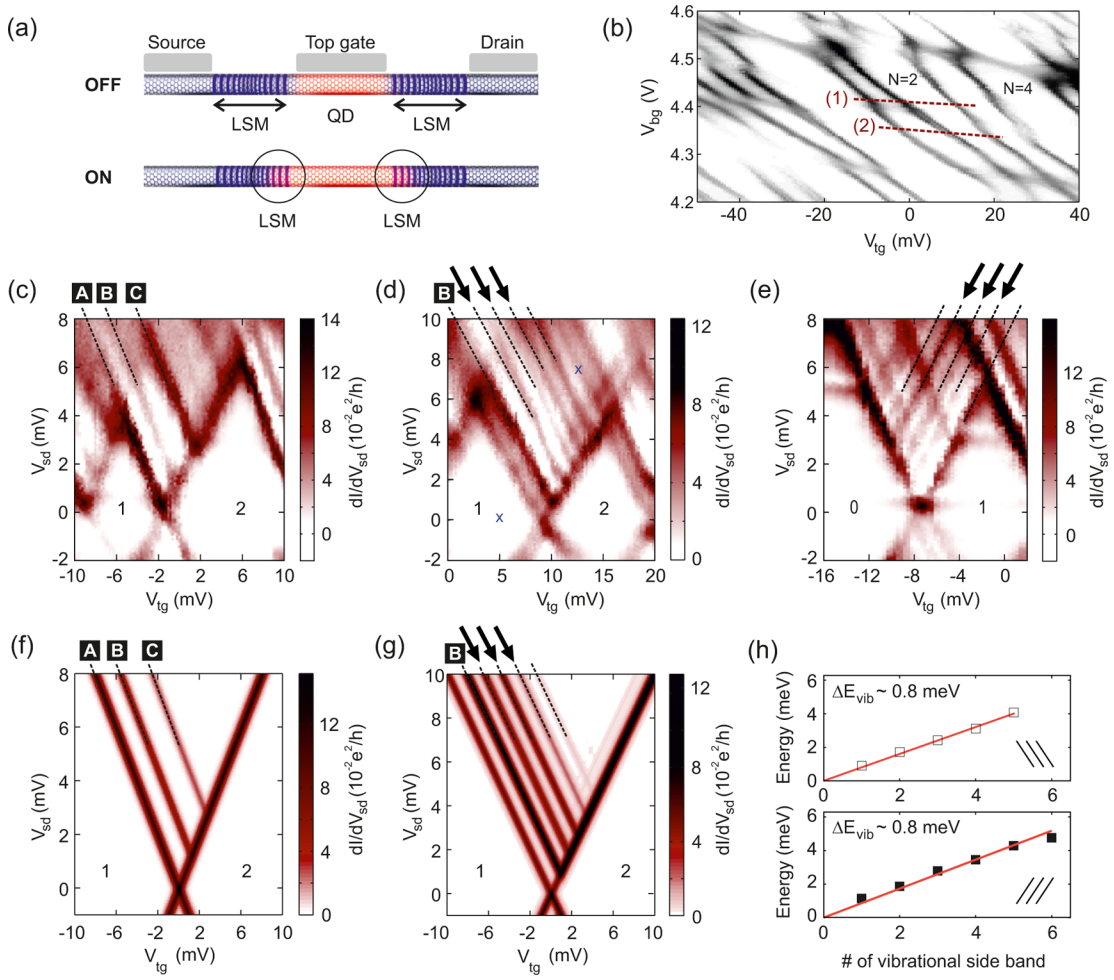

Figure 2. Switching the coupling to the vibration "on" and "off". (a) Schematic illustration of the quantum-dot tuning into a region with a longitudinal stretching mode (LSM). (b) Top- and back-gate voltage stability diagram recorded for V_{sd} = 1 mV. The lines marked (1) [V_{bg} = 4.41 V − 0.5 × V_{tg}] and (2) [V_{bg} = 4.35 V − 1.0 × V_{tg}] indicate different regimes of electron-vibration coupling. (c) dI/dV_{sd} measured along line (1) in panel (b) showing no effects of vibrations. (d) Measurement of dI/dV_{sd} along line (2) in panel (b), where significant electron-vibration coupling is observed; the arrows indicate the vibrational side bands introduced. Electronic lines A and B from panel (c) can still be identified, but C is commensurate with a vibrational sideband of B. [Note that the same happens in the calculations in panel (g).] The blue markers indicate the endpoints of the line (not shown for clarity) along which the measurements in Figure 3 are taken. (e) Similar measurement as in panel (d) but for a different relation of gate voltages (V_{tg} = 4.45 V − 0.95 × V_{bg}) showing vibrational excitations (arrows) with different gate-voltage slope, both in magnitude and sign. (f,g) Calculated dI/dV_{sd} corresponding to panel (c) and (d), respectively, see text. The overall conductance magnitude is adjusted through the coupling Γ, taking T = 0.7 K. (h) Linear fit of the vibrational excitations: the upper panel fits data from Figure 2d and the lower panel from Figure 2e, both confirming a harmonic spectrum with $\Delta E_{vib} = \hbar\omega$ = 0.8 ± 0.1 meV corresponding to 193 ± 24 GHz.

line (2), the excitation spectrum, shown in Figure 2d, changes in a way that cannot be explained by a modification of the size-quantization energy on the quantum dot: for several subsequent charge states a dense spectrum of discrete excitation peaks appears, equally spaced by $\hbar\omega$ = 0.8 ± 0.1 meV as Figure 2h shows. This is the case across the entire electronic shell that we measure, see Supporting Information. The spacing lies in the range expected for the high frequency of the longitudinal stretching mode (LSM) of the suspended parts of the CNT (length ∼65 nm as in previous studies[8,10]). Furthermore, the predominance of the excitation lines with negative slope indicates that the quantum dot couples to only one of the two suspended parts.[29,30] In Figure 2e, we demonstrate that by tuning to a different voltage regime we are able to make the other vibrating part dominate. Our system thus displays electrostatically tunable electron-vibration coupling.

To illustrate how the switchable coupling to a quantized vibration can be exploited, we now focus on measurements for the $N = 1 \leftrightarrow 2$ electron regime in Figure 2c,d. The corresponding calculations shown in Figure 2f,g are based on a quantum-dot model including the electronic states identified before in Figure 1d,e and coupling to a single vibrational mode. This model will be discussed in detail below once we have presented all experimental data. Apart from this, the non-equilibrium transport is obtained from standard master equations (see Supporting Information) that incorporate single-electron tunneling into both orbitals of the shell (with asymmetry parameter κ) from both electrodes (with junction asymmetry parameter γ). The electronic and vibrational states are assumed to relax with a phenomenological rate that exceeds the tunneling relaxation rates, taken for simplicity to be proportional to the energy change E in the transition: $\Gamma_{rel}(E) = \Gamma \times (E/0.2\ \text{meV})$. The overall tunneling rate Γ merely sets the scale of the current and is irrelevant to the relative magnitude of the different excitations which is of interest here.

DOI: 10.1021/acs.nanolett.5b00765
Nano Lett. 2015, 15, 4417−4422

To experimentally identify the electronic states to which the vibrational excitations belong, we have investigated how the differential conductance measured along the line (not shown) connecting the blue markers in Figure 2d evolves with a magnetic field B applied perpendicular to the CNT. The dominating features in Figure 3a are the vibrational sidebands

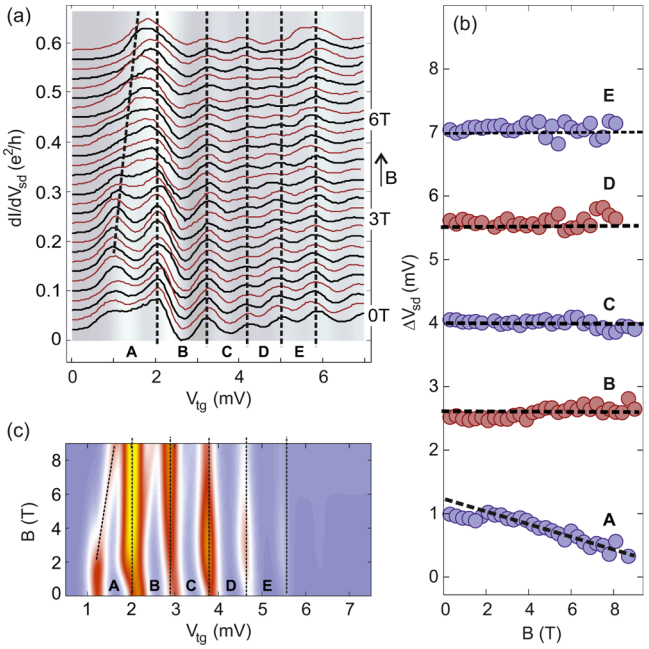

Figure 3. Magnetic field evolution of the vibrational sidebands. (a) dI/dV_{sd} as a function of top-gate voltage V_{tg} along the line (not shown) connecting the blue markers Figure 2d. Each dI/dV_{sd} line has been measured at a different magnetic field B, which has been tuned from B = 0 to 9 T in steps of 300 mT. The dI/dV_{sd} lines are offset vertically by 0.015 e^2/h for clarity. Dashed lines indicate the singlet (sloped) and triplet (vertical) transitions. (b) Bias-voltage spacings (ΔV_{sd}) of peaks A–E in panel (a) as a function of the magnetic field including additional intermediate line traces that are not shown there. The dashed line for the peak-spacing A corresponds to g-factor 2. The data are offset vertically by 1.5 mV for clarity. (c) Calculated dI/dV_{sd} evolution corresponding to panel (a).

of the lowest of the triplet excitations T_0 which in this presentation of the data appear as vertical lines. Strikingly, the ground state singlet S_- evolving with a slope has no vibrational sidebands as demonstrated by fits of the difference of the peak position in Figure 3b. This can not be explained by an Anderson–Holstein model where all electronic states with the same charge couple equally to the vibration, see Supporting Information for explicit attempts.

Instead, in our modeling we must account for state-dependent Franck–Condon shifts resulting in the vibrational potentials plotted in Figure 4. To arrive at this, we start from a model accounting for the observed set of accessible[28] many-body transport states, which is restricted by Coulomb blockade and bias voltage of a few millivolts to those shown in Figure 1e with electron numbers N = 1 and N = 2 and a single electronic K-K' shell

$$H_{el} = \varepsilon N + \Delta \sum_{\tau=\pm} \tau \sum_{\sigma} d^{\dagger}_{\tau\sigma} d_{\tau\sigma} - J\, \mathbf{S}_{+}\cdot\mathbf{S}_{-} \qquad (1)$$

Here ε is mean level position controlled by V_{tg}, Δ is the subband or valley-mixing term, and J is the exchange coupling

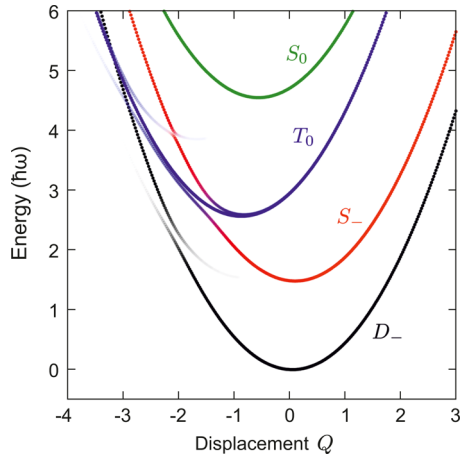

Figure 4. Vibrational potential energy surfaces underlying the quantum states of the vibrating CNT quantum dot included in the transport calculations using the same parameters as in Figures 2f,g and 3c. The excited triplet T_0 and ground singlet S_- have significantly different couplings to the vibration, that is, shifts of their potential minima relative to that of the one-electron ground state D_- strongly differ. Because of the weak SO coupling several avoided crossings can be seen. The most important anticrossing is that of the T_0 (blue) and S_- (red) potential energy surfaces. This can be understood directly from the SO operator as written in the text: it "flips" both the orbital (τ) and spin index (σ) of an electron. In Figure 1e this implies that for N = 2 the red spin up in the higher orbital is flipped into the blue spin down in the lower orbital (this represents a flip from T_0 to S_-). The resulting admixture of T_0-components (blue) to S_- (red) causes the latter to remain visible in the transport in Figure 3c with increasing the magnetic field when the tunneling becomes spin-selective due to the CNT leads. The remaining SO anticrossings are discussed in the Supporting Information, which for our parameters have negligible impact on transport.

between the spins in the two orbitals $\tau = \pm$ with spin-operators $\mathbf{S}_\tau = 1/2 \sum_{\sigma,\sigma'} d^{\dagger}_{\tau\sigma}\, \sigma_{\sigma,\sigma'} d_{\tau\sigma'}$ [σ,σ' are spin indices, σ is the usual vector of Pauli-matrices, and $d^{\dagger}_{\tau\sigma}$ creates a spin-σ electron in orbital τ]. To obtain a result as plotted in Figure 2f,g we first introduced a Holstein coupling by allowing the level position ε to depend on Q, the dimensionless vibration coordinate normalized to the zero-point motion: we thus formally replace $\varepsilon \rightarrow \varepsilon + \sqrt{2\hbar\omega\lambda_\varepsilon}Q$. This results in the commonly assumed uniform vibration coupling with strength λ_ε to all electronic states with the same charge N, which is not observed here. The required state dependent electron-vibration coupling is obtained by additionally accounting for a dependence of the other parameters on the vibration coordinate, that is, we formally replace $\Delta \rightarrow \Delta + \sqrt{2\hbar\omega\lambda_\Delta}Q$, where λ_Δ is a dimensionless one-electron valley-vibration coupling, and $J \rightarrow J + \sqrt{2\hbar\omega\lambda_J}Q$, where λ_J is a dimensionless coupling of the vibration to the two-electron exchange. Here many-body physics comes in when going from the singlet S_- ground state to the triplet T_0, the Pauli principle forces the two electrons into different orbitals which can couple differently to the vibrational mode (difference quantified by λ_Δ). However, the coupling λ_J is important as well: when allowing only for λ_Δ, the effective electronic excitation spectrum for fixed charge N (relative to which the vibration excitations are "counted") becomes dependent on the vibrational couplings (polaronic renormalization). That experimentally no significant shift of the electronic excitations is found when turning "on" the couplings to the vibration requires the couplings λ_J and λ_Δ to be

DOI: 10.1021/acs.nanolett.5b00765
Nano Lett. 2015, 15, 4417–4422

comparable in magnitude but opposite in sign. This results in an enhanced coupling of the triplet T_0 over S_- while the polaronic shifts that they induce cancel out, keeping the effective electronic excitations fixed. This thus leaves one free parameter, their magnitude, which controls the degree of state-specific coupling, which we adjust to the experiment. Together this suffices to obtain results such as Figure 2f,g that reproduce the main zero-field observations of Figure 2c,d. When the vibration couplings are "off" in Figure 2f, we estimate from Figure 2c the parameter values $\Delta = 0.8$ meV, $J = 1.5$ meV, (similar to those in Figure 1d) and use $\gamma = 0.0$, $\kappa = -0.3$. When the vibration couplings are "on" in Figure 2g, we use the same values for J and Δ but nonzero vibration couplings $\lambda_\varepsilon = 0.28$, $\lambda_\Delta = 0.32$, $\lambda_J = -0.22$, and frequency $\hbar\omega = 0.85$ meV and we adjusted the asymmetries $\gamma = -0.5$, $\kappa = 0.3$. Although there are several parameters, the experiment imposes strong restrictions, in particular, regarding the choice of vibrational couplings, excluding a simple Holstein mechanism ($\lambda_\Delta = \lambda_J = 0$), see Supporting Information. We arrive at the three electron-vibration couplings by imposing three experimental constraints after expressing the effective couplings of the electronic states in terms of λ_ε, λ_Δ, and λ_J: (i) the observed T_0-S_- splitting and (ii) S_0-T_0 splitting (commensurate with $2\hbar\omega$) should match energy expressions that depend on the vibrational couplings (polaron shift) and (iii) the vibrational-coupling of T_0 is adjusted to numerically reproduce the observed number of triplet vibrational sidebands. We note that in Figure 2d,e, the higher vibrational sidebands become more intense at high bias. As expected, this is not captured by our model because this may involve excitations beyond the lowest two electronic orbitals and energy-dependence of the tunnel barrier, neither of which we include here. We have focused instead on the nontrivial interplay of vibrational and spin-excitations for $N = 1$ and $N = 2$ in the lowest sidebands.

The resulting physical mechanism is illustrated in Figure 4: when starting out from state D_- and adding a second electron to the lowest orbital the lowest singlet state S_- experiences only a small horizontal shift of the vibrational potential minimum (both electrons in orbital $|-\rangle$ have their coupling weakened by λ_Δ and there is no spin and therefore no exchange modification of the coupling by λ_J). However, when adding the electron to the excited orbital, the coupling is not only enhanced by λ_Δ, but also by a negative λ_J when a spinfull triplet T_0 is formed. This results in a large Franck–Condon shift of the potential minimum of T_0 in Figure 4. The above horizontal shifts of the potential minima translate into suppressed vibrational sidebands for the singlet S_- and a pronounced series of sidebands for the triplet T_0, respectively (Franck–Condon effect). The presence of the further electronic states and their quantized vibrational states in Figure 4, all of which are included in our transport calculations, do not alter the above simple picture. Whereas the excited singlet S_+ does not couple to transport,[28] the role of S_0 cannot be ascertained at zero magnetic field because it is commensurate (within the line broadening) with one of the vibrational sidebands of T_0.

The field evolution in Figure 3c, calculated by adding a Zeeman term to eq 1, reproduces the main observation of Figure 3a, namely, that the triplet maintains its vibrational side bands (vertical) but the ground singlet S_- (sloped) does not. However, to obtain this agreement with the measurements we are forced to further extend the above model. First, both the excited singlet (S_0) as well as the Zeeman split-off states of the triplet (T_0) do not appear in the measurements. This we attribute to the fact that the source and drain leads of the quantum dot are not formed by metallic contacts but by small pieces of suspended CNT. Zeeman splitting of discrete states in these CNT contacts may lead to spin-filtering which turns on with the magnetic field, developing full strength at a few Tesla where $g\mu_B B \approx k_B T$. We phenomenologically account for this by a spin-dependence in tunneling to/from the electrodes which depends on B: $\zeta(B) = \tanh(g\mu_B B/2k_B T)$. Second, when only including this spin-filtering in the model, it suppresses the singlet groundstate S_- (without vibrational bands) that we do experimentally observe as excitation A in Figure 3a,b. However, when even a small spin–orbit (SO) coupling is included, the singlet S_- reappears (borrowing intensity from the triplet T_0, cf. also Figure 4), but, importantly, without reinstating the unobserved S_0 and the Zeeman split-off states of T_0 and their vibrational sidebands. This produces the observed intensity pattern, which is impossible to achieve with simple commonly used models, see Supporting Information. Here, the spin–orbit coupling is included by adding to eq 1 a term $H_{SO} = \Delta_{SO}\sum_{\sigma,\tau} d^\dagger_{\tau\sigma} d_{-\tau-\sigma}$ with $\Delta_{SO} = 0.1$ meV which allows both the spin σ and orbital index τ to be flipped in the schematic Figure 1d, thereby coupling in particular T_0 to S_-, lending it intensity. Figures 2f,g and 3c are based on the inclusion of all these effects. However, we emphasize that in the latter figure spin-filtering and spin–orbit coupling are needed exclusively to explain the missing Zeeman lines but do not lead to a qualitative change of the state-dependent coupling at $B = 0$ in Figure 2g, which is our main finding. The Supporting Information explores the influence of the various parameters, confirming the necessity of including them. The key advantage of our tunable setup is that we are able to first identify excitation A and B as relating to electronic singlet S_- and triplet T_0, respectively, and subsequently allowing us to study the vibrational sidebands C-E.

In conclusion, we have demonstrated switchable coupling of a quantized vibration of a carbon nanotube to its quantized electronic states. Using this advance we explored the two-electron regime, including the magnetic field dependence, and found indications of state-dependent vibrational transport sidebands not described by standard models. We showed that the interplay of intrinsic effects on the carbon nanotube (Coulomb blockade, valley-index, and spin-exchange) and experimental details (junction, orbital, and spin asymmetries) can explain the observations. This, however, includes vibrational couplings that involve internal spin- and valley-degrees of freedom, bringing spin- and valley-tronics physics within range of NEMS.

■ ASSOCIATED CONTENT

Supporting Information

Fabrication and experimental characterization of the quantum dot, the electrostatic control of the coupling to vibrational modes, and theoretical analysis of the electronic and vibrational quantum states of the model and the transport calculations using master equations. This material is available free of charge via the Internet at http://pubs.acs.org/.The Supporting Information is available free of charge on the ACS Publications website at DOI: 10.1021/acs.nanolett.5b00765.

■ AUTHOR INFORMATION

Corresponding Author

*E-mail: stampfer@physik.rwth-aachen.de.

DOI: 10.1021/acs.nanolett.5b00765
Nano Lett. 2015, 15, 4417–4422

Author Contributions

P.W. and H.L.C. contributed equally.

Notes

The authors declare no competing financial interest.

■ ACKNOWLEDGMENTS

We acknowledge F. Cavaliere for stimulating discussions and S. Trellenkamp and J. Dauber for support with sample fabrication. We acknowledge support from the Helmholtz Nanoelectronic Facility (HNF) and financial support by the JARA Seed Fund and the DFG under Contract No. SPP-1243 and FOR912.

■ REFERENCES

(1) Moser, J.; Güttinger, J.; Eichler, A.; Esplandiu, M. J.; Liu, D. E.; Dykman, M. I.; Bachtold, A. *Nat. Nanotechnol.* **2013**, *8*, 493.
(2) Teufel, J. D.; Donner, T.; Castellanos-Beltran, M. A.; Harlow, J. W.; Lehnert, K. W. *Nat. Nanotechnol.* **2009**, *8*, 820.
(3) Viennot, J. J.; Delbecq, M. R.; Dartiailh, M. C.; Cottet, A.; Kontos, T. *Phys. Rev. B* **2014**, *89*, 165404.
(4) Schneider, B.; Etaki, S.; van der Zant, H.; Steele, G. *Sci.Rep.* **2012**, *2*, 599.
(5) Park, H.; Park, J.; Lim, A. K. L.; Anderson, E. H.; Alivisatos, A. P.; McEuen, P. L. *Nature* **2000**, *407*, 57.
(6) Pasupathy, A. N.; Park, J.; Chang, C.; Soldatov, A. V.; Lebedkin, S.; Bialczak, R. C.; Grose, J. E.; Donev, L. A. K.; Sethna, J. P.; Ralph, D. C.; McEuen, P. L. *Nano Lett.* **2005**, *5*, 203.
(7) Osorio, E. A.; O'Neill, K.; Stuhr-Hansen, N.; Nielsen, O. F.; Bjørnholm, T.; van der Zant, H. S. J. *Adv. Mater.* **2007**, *19*, 281.
(8) Sapmaz, S.; Jarillo-Herrero, P.; Blanter, Y.; Dekker, C.; van der Zant, H. S. J. *Phys. Rev. Lett.* **2006**, *96*, 026801.
(9) Steele, G. A.; Hüttel, A. K.; Witkamp, B.; Poot, M.; Meerwaldt, H. B.; Kouwenhoven, L. P.; van der Zant, H. S. J. *Science* **2009**, *325*, 1103.
(10) Leturcq, R.; Stampfer, C.; Inderbitzin, K.; Durrer, L.; Hierold, C.; Mariani, E.; Schultz, M. G.; von Oppen, F.; Ensslin, K. *Nat. Phys.* **2009**, *5*, 317.
(11) Pei, F.; Laird, E. A.; Steele, G. A.; Kouwenhoven, L. P. *Nat. Nanotechnol.* **2012**, *7*, 630.
(12) Benyamini, A.; Hamo, A.; Viola Kusminskiy, S.; von Oppen, F.; Ilani, S. *Nat. Phys.* **2014**, *10*, 151.
(13) Moser, J.; Eichler, A.; Güttinger, J.; Dykman, M. I.; Bachtold, A. *Nat. Nanotechnol.* **2014**, *9*, 1007.
(14) Ohm, C.; Stampfer, C.; Splettstoesser, J.; Wegewijs, M. R. *Appl. Phys. Lett.* **2012**, *100*, 143103.
(15) Pa'lyi, A.; Struck, P. R.; Rudner, M.; Flensberg, K.; Burkard, G. *Phys. Rev. Lett.* **2012**, *108*, 206811.
(16) Kuemmeth, F.; Ilani, S.; Ralph, D. C.; McEuen, P. L. *Nature* **2008**, *452*, 448.
(17) Jespersen, T.; Grove-Rasmussen, K.; Paaske, J.; Muraki, K.; Fujisawa, T.; NygÅrd, J.; Flensberg, K. *Nat. Phys.* **2011**, *7*, 348.
(18) Flensberg, K.; Marcus, C. M. *Phys. Rev. B* **2010**, *81*, 195418.
(19) Sazonova, V.; Yaish, Y.; Ustunel, H.; Roundy, D.; Arias, T. A.; McEuen, P. L. *Nature* **2004**, *431*, 284.
(20) Eichler, A.; del Álamo Ruiz, M.; Plaza, J. A.; Bachtold, A. *Phys. Rev. Lett.* **2012**, *109*, 025503.
(21) Barnard, A. W.; Sazonova, V.; van der Zande, A. M.; McEuen, P. L. *Proc. Natl. Acad. Sci. U.S.A.* **2012**, *109*, 19093.
(22) Palomaki, T. A.; Teufel, J. D.; Simmonds, R. W.; Lehnert, K. W. *Science* **2013**, *342*, 710.
(23) Ganzhorn, M.; Klyatskaya, S.; Ruben, M.; Wernsdorfer, W. *Nat. Nanotechnol.* **2013**, *8*, 165.
(24) Pa'lyi, A.; Burkard, G. *Phys. Rev. Lett.* **2011**, *106*, 086801.
(25) Liang, W.; Bockrath, M.; Park, H.-K. *Phys. Rev. Lett.* **2002**, *88*, 126801.
(26) Buitelaar, M. R.; Nussbaumer, T.; Iqbal, M.; Schönenberger, C. *Phys. Rev. Lett.* **2002**, *88*, 156801.
(27) Sapmaz, S.; Jarillo-Herrero, P.; Kong, J.; Dekker, C.; Kouwenhoven, L. P.; van der Zant, H. S. J. *Phys. Rev. B* **2005**, *71*, 153402.
(28) In this state two electrons fill the excited orbital causing the amplitude for a transition from the $N = 1$ ground state with an electron in the ground orbital to be strongly suppressed. For this transition to happen, one must shuffle the lower electron up and add another electron, something which is only possible for very strong spin−orbit coupling or higher-order tunnel processes, neither of which are relevant here. This point is important since due to polaronic renormalization discussed at the end of the letter S_+ may actually lie below S_0 but even then it cannot be observed.
(29) Cavaliere, F.; Mariani, E.; Leturcq, R.; Stampfer, C.; Sassetti, M. *Phys. Rev. B* **2010**, *81*, 201303.
(30) Donarini, A.; Yar, A.; Grifoni, M. *New. J. Phys.* **2012**, *14*, 023045.

DOI: 10.1021/acs.nanolett.5b00765
Nano Lett. 2015, 15, 4417−4422